Smart Structures and Systems, Vol. 11, No. 4 (2013) 365-386
DOI: http://dx.doi.org/10.12989/sss.2013.11.4.365

Bridge deflection evaluation using strain and rotation measurements

Helder Sousa*[1], Filipe Cavadas[1], Abel Henriques[1], João Bento[2] and Joaquim Figueiras[1]

[1]*LABEST, Faculdade de Engenharia, Universidade do Porto, Rua Dr. Roberto Frias s/n, 4200-465 Porto, Portugal*
[2]*Department of Civil Engineering and Architecture, Instituto Superior Técnico, 1049-001 Lisboa, Portugal*

(Received October 3, 2011, Revised June 17, 2012, Accepted October 27, 2012)

Abstract. Monitoring systems currently applied to concrete bridges include strain gauges, inclinometers, accelerometers and displacement transducers. In general, vertical displacements are one of the parameters that more often need to be assessed because their information reflects the overall response of the bridge span. However, the implementation of systems to continuously and directly observe vertical displacements is known to be difficult. On the other hand, strain gauges and inclinometers are easier to install, but their measurements provide no more than indirect information regarding the bridge deflection.
In this context, taking advantage of the information collected through strain gauges and inclinometers, and the processing capabilities of current computers, a procedure to evaluate bridge girder deflections based on polynomial functions is presented. The procedure has been implemented in an existing software system – MENSUSMONITOR –, improving the flexibility in the data handling and enabling faster data processing by means of real time visualization capabilities. Benefiting from these features, a comprehensive analysis aiming at assessing the suitability of polynomial functions as an approximate solution for deflection curves, is presented. The effect of boundary conditions and the influence of the order of the polynomial functions on the accuracy of results are discussed. Some recommendations for further instrumentation plans are provided based on the results of the present analysis. This work is supported throughout by monitoring data collected from a laboratory beam model and two full-scale bridges.

Keywords: bridge monitoring; deflection evaluation; strain gauges; inclinometers; polynomial fitting

1. Introduction

Structural monitoring has been subject to increasing interest within the scientific and technical communities. At the same time, Bridge Health Monitoring Systems (BHMS) have been applied more intensively worldwide. Firstly, attention was focussed on sensors applications. However, the emphasis has recently been shifted to the practical implications regarding acquisition, storage and data processing (Van der Auweraer and Peeters 2003). Presently, it is possible to monitor, continuously and remotely, extensively instrumented structures with a high degree of automation. Present solutions are versatile enough to carry out remote surveillance tasks with moderate costs

*Corresponding author, E-mail: mail@ hfmsousa.com

(BRITE/EURAM 1997, Van der Auweraer and Peeters 2003).

In recent years, the concept of "smart structures" has increasingly been attracting the interest of the civil engineering community (BRITE/EURAM 1997). Full-scale structures equipped with sensors, processing units and communication networks are a reality all over the world, and these complex systems might become a powerful instrument to support the surveillance and maintenance tasks inherent to bridges.

Current monitoring systems applied to concrete bridges consist of strain gauges to measure local deformation, inclinometers to measure rotations, accelerometers to measure accelerations and displacement transducers to measure bearing displacements. Vertical displacements are one of the parameters that more often need to be monitored for short and long-term observation. Bridge deflections reflect the overall response of the structure providing essential information about the performance in service. However, it is well known how difficult it is to implement a measuring setup to observe vertical displacements in a bridge. The current solutions, available in the market, to measure vertical displacements are often difficult to use and require specialized operators. For example, traditional transducers need a reference base and are not suitable for several situations, e.g., on a river-bed. One of the most widely used methods to measure vertical displacements on a river-bed is the levelling system. However, it has disadvantages, such as the possible loss of reference marks and its cost in comparison with other methods. Attempts have been made to apply GPS technology to monitor displacements, however, these approaches are still far from being either accurate enough or effective. Therefore, there is a need for an alternative and expeditious approach to determine vertical displacements in bridges.

Strain gauges and inclinometers are easier to install than systems to measure vertical displacements. Nonetheless, deformations and rotations are indirect information about bridge deflection. Taking advantage of the data collected with these sensors and the processing capabilities of the current computers, some authors have tried to estimate vertical displacements based on concrete deformations and rotations. Vurpillot et al. presented one of the first attempts to estimate vertical displacements using measurements collected by strain gauges and inclinometers (Vurpillot *et al.* 1998). Considering the Bernoulli beam theory, the authors present a formulation based on a polynomial function to approximate the beam deflection. The strain and rotation measurements worked as constraints to the polynomial function. The methodology was tested in a laboratorial load test and on a full-scale bridge under daily temperature variations during 24 hours. A similar application, in which only strains are used, is presented in (Chung *et al.* 2008). A prestressed concrete girder was instrumented with long optical strain gauges, and using the geometric relation between curvature and vertical deflection in a simple beam the deflection curve of the girder was estimated. Analogously, Hou *et al*. used only measurements of inclinometers to estimate the bridge deflection (Hou *et al.* 2005). Another example of estimating bridge deflection based on measurements of inclinometers can be found in (Burdet and Zanella 2000).

Considering these previous studies, the aim of this work is to demonstrate the suitability of the polynomial approach to estimate the deflection curve of full-scale concrete bridges. Measurements obtained from monitoring systems devoted to surveillance and maintenance, composed mainly of inclinometers over the supports and strain gauges at mid-span and near the supports, are used. Moreover, these measurements are concerned with short-term observations obtained during load tests. An automatic procedure was developed and implemented in software devoted to the management, treatment and analysis of monitoring results − MENSUSMONITOR (Sousa *et al.* 2008). This option improves data handling, with the possibility of real time visualization. Firstly, the main steps of the procedure to estimate bridge deflections are presented. After that, their

application to a prestressed concrete beam is carried out in order to appraise its performance in laboratory conditions. Afterwards, the results obtained for two full-scale bridges – Sorraia Bridge and Lezíria Bridge – are shown and discussed in detail. In order to evaluate the suitability of polynomial functions as an approximate solution for deflection curves, a comprehensive analysis was carried out. The focus was not limited to the effect of the boundary conditions, but to the effect of the order of the polynomial functions on the results' accuracy. Finally, a set of relevant conclusions are reported regarding the optimization of monitoring plans with the aim of estimating bridge deflections based on strain-gauge and inclinometer measurements.

2. Procedure to estimate bridge deflections

2.1 Introduction

For a period between $t_{initial}$ and t_{final}, a database with a set of experimental registers is assumed, where each register contains the measurements performed by a set of sensors. This database contains measurements of concrete deformations and rotations of the most critical cross-sections of the bridge girder. These critical cross-sections – S_i, i = 1, 2..., n – are generally located at the mid-span and near the bridge supports (Fig. 1).

During the operational life, a linear elastic behaviour is expected and therefore, the bridge deflection might be accurately estimated with simple mathematical models.

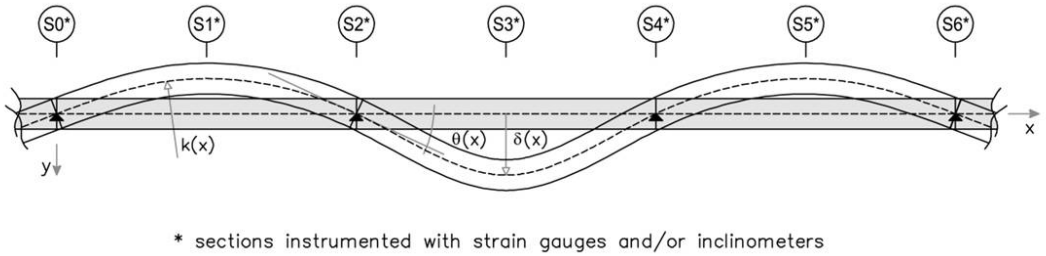

Fig. 1 Bridge deflection based on the monitoring of instrumented cross-sections

Considering the Bernoulli hypothesis – plane sections after deformation – the deflection curve of a uniformly loaded beam of 'm' spans is expressed as a sequence of 'm' fourth degree polynomials, $P_j^4(x)$. Each span is considered with constant inertia, uniformly loaded, and subjected to end forces and moments (Massonnet 1968). However, for full-scale bridges, material properties as well as the cross-section may vary along its length. Furthermore, the Bernoulli hypothesis is not valid either near the supports or in areas where concentrated loads are applied. Therefore, the function that expresses the bridge deflection is actually rational, namely because of the variability of the mechanical properties and the cross-section inertia along the bridge length.

Nevertheless, for moderate loads, the bridge deflection is a smooth curve, where the vertical displacements are considerably low if compared with the length of span, even for failure scenarios. Hence, the approximation of the bridge deflection with a polynomial function is reasonable.

The procedure adopted herein calculates a polynomial function based on two types of information previously known: (i) intrinsic characteristics of the bridge's behaviour, namely zero

vertical displacement over the supports, and null curvature over the outer supports and (ii) curvatures and rotations based on measurements respectively performed with strain gauge and inclinometer sensors. In this context, the problem is solved according to the following steps.

2.2 Calculation steps

2.2.1 Section curvature

The curvature, $\kappa(x)$, is a function of the bridge deflection, $\delta(x)$, as expressed by Eq. (1) (Massonnet 1968). As aforementioned, if compared with the beam length, the vertical displacements are generally very small and consequently, for $d\delta(x)/dx$ small values are attained. Therefore, the value of $(d\delta(x)/dx)^2$ can be neglected and the denominator of Eq. (1) becomes unitary, so that the curvature might be expressed by Eq. (2).

$$\kappa(x) = \frac{\dfrac{d^2\delta(x)}{dx^2}}{\left[1+\left(\dfrac{d\delta(x)}{dx}\right)^2\right]^{3/2}} \Leftrightarrow \tag{1}$$

$$\Leftrightarrow \kappa(x) = \frac{d^2\delta(x)}{dx^2} \quad , \quad \left(\frac{d\delta(x)}{dx}\right)^2 \cong 0 \quad \textit{for small displacements} \tag{2}$$

For pure bending, the neutral axis is known a priori, and the curvature of a cross-section can be calculated with Eq. (3), where $\varepsilon(x)$ represents the deformation of the fibre at distance 'y' from the neutral axis.

$$\kappa(x) = \frac{\varepsilon(x)}{y} \tag{3}$$

However, if the beam is not restricted to bending, the curvature can be calculated based on the deformations of two different fibres. This can be achieved by using appropriate strain gauges placed in the bottom and top fibres, denoted as, SG-bot and SG-top, respectively (Fig. 2). Afterwards, the curvature of the instrumented cross-section can be calculated by Eq. (4), where H represents the distance between those two fibres.

$$\kappa(x) = \frac{\varepsilon_{bot}(x) - \varepsilon_{top}(x)}{H(x)} \tag{4}$$

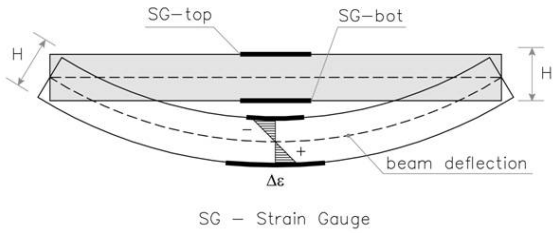

Fig. 2 Calculation of the cross-section curvature based on strain gauges measurements

As expressed by Eq. (5), a second-order constraint of the deflection curve is set by replacing Eq. (4) in Eq. (2). In other words, strain gauges allow the calculation of curvature, which might be used as a second-order boundary constraint for the polynomial function.

$$\frac{d^2\delta(x)}{dx^2} = \frac{\varepsilon_{bot}(x) - \varepsilon_{top}(x)}{H(x)} \tag{5}$$

2.2.2 Section rotation

The relation between the deflection curve, $\delta(x)$, and the rotation $\theta(x)$ is expressed by Eq. (6). However, the rotation of any cross-section is considerably small, normally in the order of 10^{-3} of a degree, due to the small magnitude of the vertical displacements as aforementioned. Therefore, Eq. (6) might be simplified to Eq. (7), and the rotations can be directly used as a first-order constraint for the polynomial function.

$$\theta(x) = arctg\left[\frac{d\delta(x)}{dx}\right] \Leftrightarrow \tag{6}$$

$$\Leftrightarrow \theta(x) = \frac{d\delta(x)}{dx}, \quad for\ small\ rotations \tag{7}$$

2.2.3 Polynomial function setting

A polynomial function is set for each span, which means that '*m*' polynomials are calculated for the '*m*' bridge spans. This option allows a flexible *modus operandi* in the data handling and the required versatility to apply on bridges with a large number of spans. The process is repeated '*m*' times through a *while-loop*. The polynomial function is calculated based on boundary constraints.

Fig. 3 shows a generic bridge span and its deflection, highlighting the constraints at mid-span and support cross-sections. However, some constraints may not exist for real cases, depending on the instrumentation available for each span.

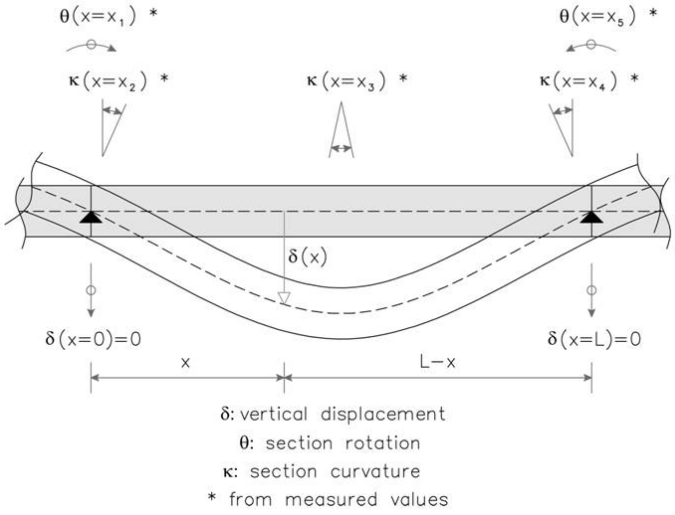

Fig. 3 Span deflection and boundary constraints

For a generic span j, if '$n+1$' boundary constraints are known, an 'n' degree polynomial function, $P_j^n(x)$, as expressed by Eq. (8), can be fitted to obtain the vertical displacement $\delta_j(x)$. For the generic case presented in Fig. 3, seven boundary constraints are known and a 6th order polynomial function can be defined, which is the maximum degree that the polynomial function can attain. If compared with a unique polynomial function for the entire length of the bridge, using a polynomial function for each span leads to lower degree polynomial functions and therefore, problems of overfitting are avoided (Björck 1996).

$$\delta_j(x) \cong P_j^n(x) = \sum_{p=0}^{n} c_{j,p} \cdot x^p \quad , \quad j-span \tag{8}$$

The polynomial coefficients $c_{j,p}$, in Eq. (8) are the unknowns, which are calculated considering the abovementioned boundary constraints, namely: (i) null vertical displacements over the supports and null curvatures over the outer supports; (ii) curvatures and rotations derived from the sensor readings. Therefore, with the '$n+1$' boundary constraints known for the generic span 'j', a system of linear equations can be set as expressed by Eq. (9) in matrix notation.

$$[A]_j \cdot \{c\}_j = \{b\}_j \tag{9}$$

The matrix $[A]$ depends on the span geometry, namely, the location of the instrumented cross-sections, x_i, and the span length, L. The span length dependence is only due to numerical aspects. The cross-section location is normalized to x/L, which limit the possible locations from zero to one. In this context, the matrix coefficients are more homogeneous and potential instability in the matrix inversion is prevented. The vector $\{c\}_j$ contains the problem unknowns − the polynomial coefficients − and the vector $\{b\}_j$ the boundary constraints. The problem solution is given by Eq. (10), for which it must be assured that the matrix $[A]$ is not singular. This can be assured by considering linearly independent constraints.

$$\{c\}_j = [A]_j^{-1} \cdot \{b\}_j \tag{10}$$

2.2.4 Calculation of the bridge deflection shape

Finally, the vertical displacements, δ, are calculated for a set of cross-sections (1,2, …, z), in order to arrive at the deflection shape. At this stage, the polynomial functions are perfectly known and therefore, the vertical displacement can be calculated using Eq. (11) for any bridge cross-section, $S_{x=x_k}$, by solving $P(x = x_k)$. Moreover, rotations, θ, and curvatures, κ, can also be calculated by simply taking the derived functions $P'(x = x_k)$ and P'' $(x = x_k)$ as expressed, respectively, by Eqs. (12) and (13).

$$\delta: \; P_j(x_k) = \sum_{p=0}^{n} c_{j,p} \cdot x_k^p \quad , \quad k = 1,2,...,z \tag{11}$$

$$\theta: \; P_j'(x_k) = \sum_{p=1}^{n} p \cdot c_{j,p} \cdot x_k^{p-1} \quad , \quad k = 1,2,...,z \tag{12}$$

$$\kappa: \; P_j''(x_k) = \sum_{p=2}^{n} p \cdot (p-1) \cdot c_{j,p} \cdot x_k^{p-2} \quad , \quad k = 1,2,...,z \tag{13}$$

2.3 Software implementation

The aforementioned calculation steps were implemented in an existing piece of software, specifically devoted to the treatment, processing and analysis of data concerning the Structural Health Monitoring of bridges – MENSUSMONITOR (Sousa *et al.* 2008). Data access through database consulting and data pre-treatment, as well as real-time visualization capabilities, are features already available in this software. Therefore, the implementation in this software makes its application easier and faster when compared with usual commercial tools such as spreadsheets.

Moreover, the calculation steps can be automatically extended, by a temporal cycle, for an observation period $[t_{\text{initial}},t_{\text{final}}]$, where a generic register, occurred at instant t, contains all sensor measurements, namely deformations, ε, and rotations, θ. Fig. 4 presents a flowchart of the calculation steps within a temporal cycle.

2.4 Validation on a simply supported beam

The procedure was first assessed on a simply supported prestressed concrete beam with a 150 mm × 200 mm cross-section and an effective span of 3.96 m (Fig. 5). A concrete of class C40/50 and steel of class S500 were used. The longitudinal reinforcement consists of 4ϕ12 mm, while for the transversal direction the reinforcement is set by 2ϕ6 mm 10 cm spaced. Additionally, the beam was prestressed with a force of 172 kN, by using a seven-wire strand with a 1.40 cm^2 cross-section and yield stress of 1857 MPa (Sousa 2002).

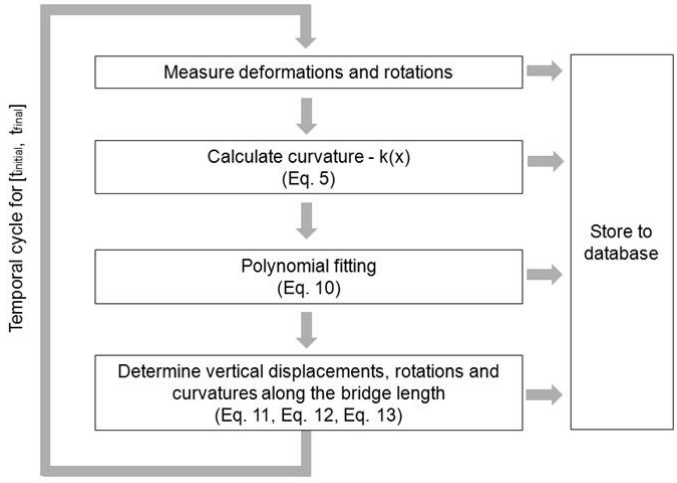

Fig. 4 Flowchart of the calculation steps

As illustrated in Fig. 5, three cross-sections, S1, S2 and S3, are monitored with six electric

strain gauges each, two sensors being embedded into concrete (CD) and the remaining four bonded to the reinforcement bars (SD). Additionally, the vertical displacements on cross-sections SA, SB and SC were measured with LVDT's, and the rotations at the two end cross-sections were also measured using electric inclinometers. The environmental temperature was also measured. An automatic acquisition system was provided to collect and register the values measured by all sensors (Sousa 2002, Cavadas *et al.* 2009).

The beam was loaded on cross-sections SA and SC with two point loads, F1 and F2, respectively (Fig. 5). Table 1 summarizes the two load cases considered for this work, each one as a combination of loads F1 and F2. The condition of L/2000 was established as the maximum deflection in order to ensure elastic behaviour during the tests.

Fig. 6 plots the results obtained, in which the vertical displacements measured with LVDT's (grey circles) and the beam deflections calculated with the polynomial function (black line) are overlapped. A 4th degree polynomial function was used, based on the null vertical displacements and the measured rotations at the beam-ends and the curvature at cross-section S2. A good conformity between the polynomial function and the measurements was achieved for both load cases, with a maximum error of + 2.1% in cross-section SA (Fig. 6(a)) and - 4.9% in cross-section SB (Fig. 6(b)) for LC1 and LC2, respectively. Nevertheless, it should be noted that the experimental tests were conducted with a different purpose (Cavadas *et al.* 2009).

Table 1 Load cases (kN)

Load Case	F1	F2
LC1	4.42	0.19
LC2	0.97	3.79

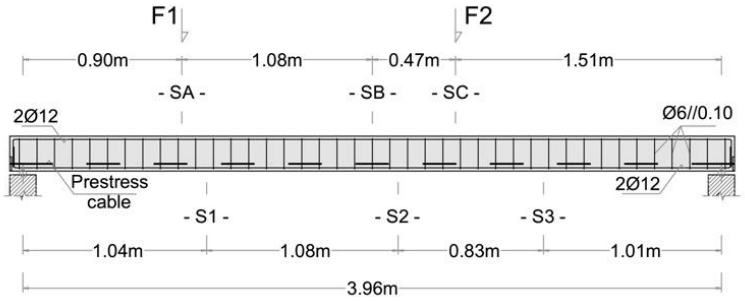

(a) elevation

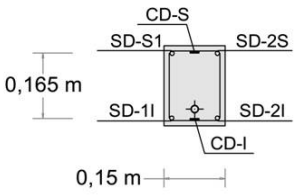

(b) cross-section (S1, S2 and S3)

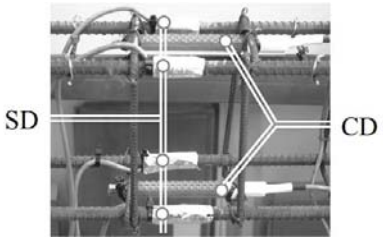

(c) sensors' installation

Fig. 5 Simply supported prestressed concrete beam

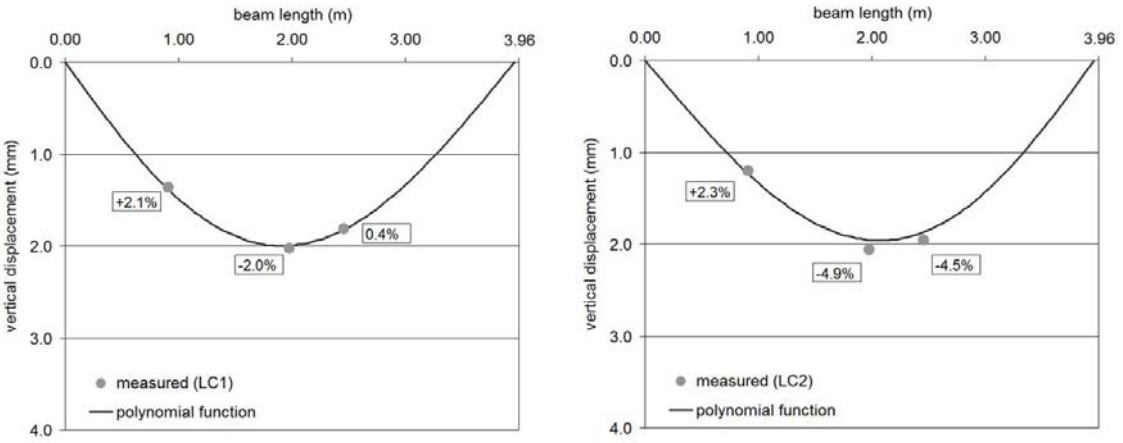

(a) LC1 (b) LC2

Fig. 6 Beam deflections for two different load cases

3. Full-scale applications

3.1 Introduction

The deflection of a bridge span is highly influenced by the behaviour of cross-sections near the mid-span and support zones. Moreover, a failure scenario normally starts in these zones due to the high strain level. Generally, higher curvatures are measured in cross-sections near the mid-spans and support zones, while for rotations, the higher values are measured for cross-sections close to the deck supports.

Two bridges − Sorraia Bridge and Lezíria Bridge − provided with monitoring systems were subject to analysis to evaluate the presented procedure in full-scale structures. These structures are part of two important motorways in Portugal. The monitoring systems were designed to aid the surveillance and maintenance operations. The vertical displacements were measured only at the mid-span cross-sections. However, in order to get a more comprehensive insight into the bridge deflection, this analysis is also supported by results obtained from numerical models, which were developed based on finite element techniques. Therefore, the estimated vertical displacements can be confronted, not only in the cross-sections where the measurements were taken, but also throughout the bridge length taking advantage of the results from the numerical models. With this strategy, the results obtained from the polynomial functions can be analysed and discussed more accurately.

3.2 Sorraia Bridge

Sorraia Bridge, which is situated at Salvaterra de Magos as part of the Portuguese A13 motorway, is a prestressed concrete bridge with two parallel and identical structures – east and west bridges with a total length of 1,666 m each (Fig. 7). Focussing on the main bridge of the east side, this structure, with a total length of 270 m, was constructed using the balanced cantilever method. The structure has three spans, two end spans of 75 m length and a central span of 120 m length (Fig. 8). The bridge deck is a box girder whose height ranges between 2.55 m, at mid-span,

and 6.00 m at the support zone, and is supported on piers 7.50 m height through unidirectional bearings. Pilecaps of five piles, each one with 2.0 m diameter and 30 m long, support each pier.

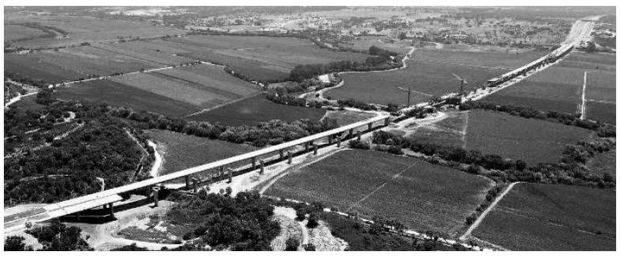

Fig. 7 Sorraia Bridge

As aforesaid, a long-term monitoring system was installed in the east deck of Sorraia Bridge, which was set up under the scope of a consortium project between *BRISA − Auto-Estradas de Portugal, S.A.* and two R&D institutions, *LABEST-FEUP* and *INESC-PORTO*, and partially funded by *AdI – Innovation Agency* (Perdigão 2006). Long-term observation of the bridge's behaviour started in the early construction phase. The main instrumentation is based on strain-gauges that encapsulate simultaneously electric and optical sensors (Fig. 9(a)) (Sousa 2006) and temperature sensors, in a set of cross-sections. The environmental temperature and relative humidity, inside and outside the box girder (Fig. 9(b)), are also monitored. In addition, a temporary monitoring system was provided during the load test, to observe other important parameters, namely, vertical displacements and rotations. Further, data collected by this temporary system was very useful to assess the bridge's behaviour as well as to evaluate the performance of the permanent monitoring system through cross analysis of data. Fig. 8 and Table 2 illustrate and detail the monitoring plan for this case.

Focussing the assessment of the bridge's behaviour during the load test, a numerical model was built based on finite element techniques. The effective properties of the applied materials and the loads applied during the load test were taken into consideration. Moreover, a two-dimensional beam model, in accordance with the Timoshenko theory, was developed to simulate the concrete elements of the bridge, which is a reasonable approach to analyse the overall behaviour of the bridge.

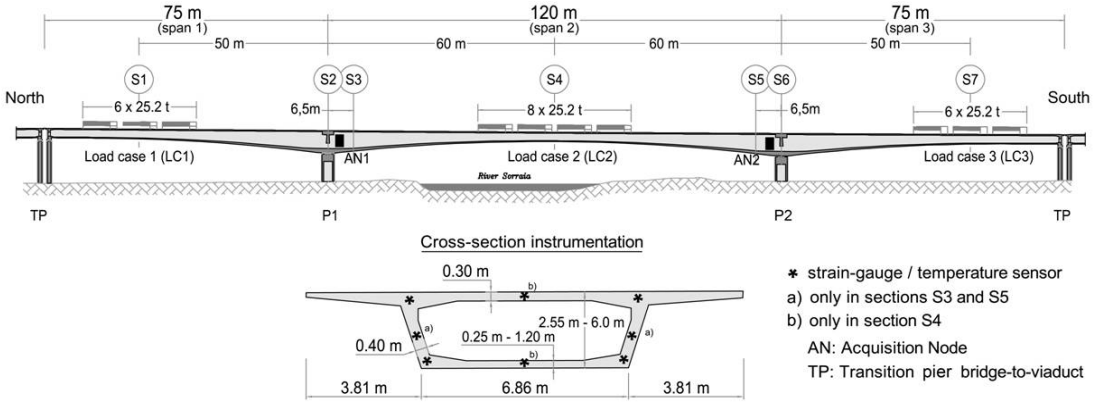

Fig. 8 Location of the instrumented cross-sections in Sorraia Bridge

The assessment of the vertical displacements with the stated procedure was made based on measurements collected during the load test that was performed at the end of construction. Without puting the bridge's elastic behaviour at risk, trucks, fully loaded and of controlled weight were used to carry out the load tests. These tests comprised a set of configurations with the trucks immobilized at specific positions of the bridge. Among all configurations, three load cases, Load Case 1, 2 and 3 that explored the maximum curvature of the three mid-span cross-sections (Fig. 8), are considered for this work.

The polynomial functions were calculated based on the measurements and the intrinsic characteristics of the bridge, namely null vertical displacements above piers and null curvature at the end support of the outer spans (span 1 and span 3).

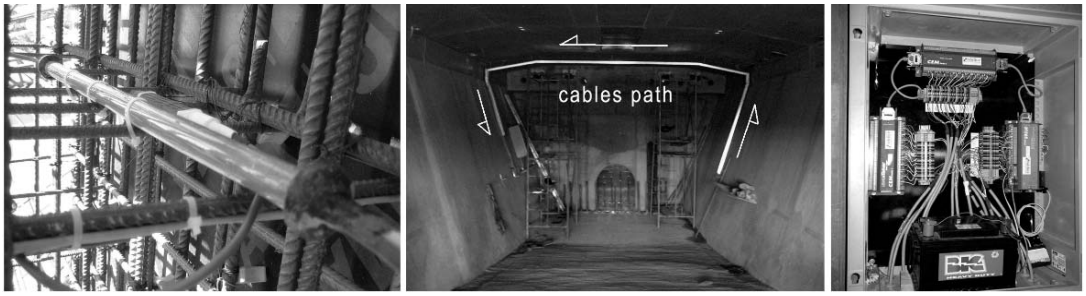

(a) Electric/Optical strain-gauge (b) Interior of the box-girder (c) Acquisition Node

Fig. 9 Monitoring system of Sorraia Bridge

Table 2 Instrumentation typology and quantities – Sorraia Bridge

Parameter	S1	S2	S3	S4	S5	S6	S7
Vertical displacement	1	-	-	1	-	-	1
Rotation	-	1	-	-	-	1	-
Deformation	4	-	6	6	6	-	4
Temperature	-	-	-	-	2	-	-

Fig. 10(a) shows the vertical displacements obtained for the three load cases, namely the measured values (bullet points), the deflection curves using the polynomial functions (continuous lines) and those obtained with the numerical model (dashed lines). In addition, the relative errors are also presented (text boxes), for which the measured value was taken as reference. Comparing the predicted values with the measured ones, the best result occurs in cross-section S4, which was obtained with a 6^{th} degree polynomial function. In contrast, the use of a 4^{th} degree polynomial function led to poorer results for span 1 and 3. This result was already expected due to the higher number of instrumented cross-sections in span 2 (Fig. 8). The error, lower than 1%, obtained for cross-section S4 is a good indicator, taking into account that the real span deflection is not rigorously interpreted by a polynomial function. However, for spans 1 and 3, the relative errors for cross-sections S1 and S7 are greater than 10%. This decrease in the quality of the results can be explained by the different constraints available for these spans, namely for the span ends, for which only one curvature and one rotation is known. This contrasts with the knowledge of the rotations and curvatures at both ends of span 2 (Fig. 8). For a better understanding of the results,

Fig. 10(b) presents the rotation diagrams obtained by the procedure, according to Eq. (12), and the corresponding ones obtained by the numerical model. The higher deviations are clearly seen for zones near the piers P1 and P2. Particularly for LC1 and LC3, higher rotations in cross-sections of spans 1 and 3 near the piers P1 and P2 are computed by the polynomial functions. This leads to higher displacements in these zones, which influence and overestimate the spans' deflection.

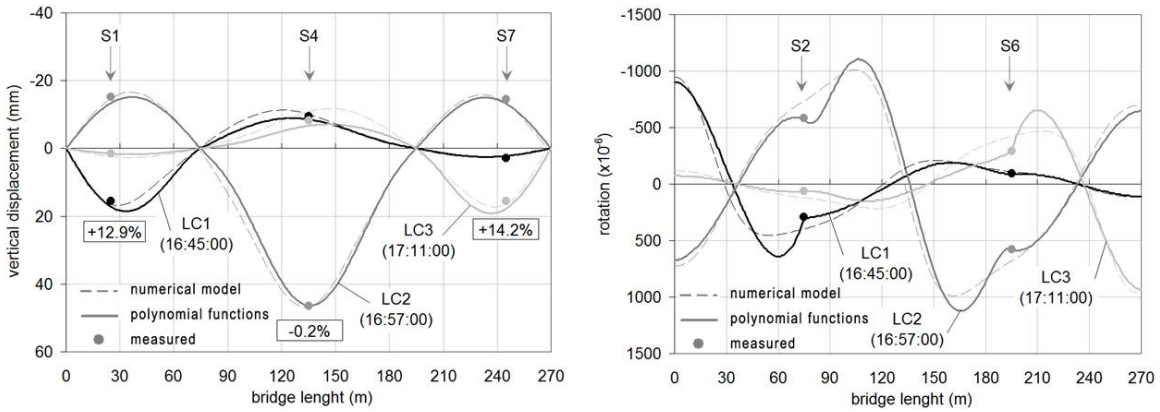

(a) vertical displacement diagrams (b) rotation diagrams

Fig. 10 Sorraia Bridge results for LC1, LC2 and LC3 (case 0)

3.3 Lezíria Bridge

Lezíria Bridge is part of the A10 motorway in Portugal. With a total length of 39.9 km, this motorway is an outer periphery bound to the Lisbon Metropolitan Area. The main bridge structure has a total length of 970 m (Fig. 11), with eight spans of 95 + 127 + 133 + 4×130 + 95 m length, respectively, and seven piers supported by pilecaps over the riverbed (Fig. 12). The bridge deck is a box girder with variable inertia - approximately 30.00 m wide and height raging from 4.00 m to 8.00 m. The box girder core was segmentally built using a movable scaffolding system, while the side cantilevers were subsequently constructed with a specific movable scaffolding and metallic struts fixed on the bottom slab of the box girder. The concrete piers are formed by four walls with constant thickness and variable width and supported by pilecaps.

Fig. 11 Lezíria Bridge − construction stage in May 2007

The bridge has an integrated monitoring system devoted to the management and surveillance of the structure (Sousa *et al.* 2011). Several cross-sections are instrumented with embedded and external sensors that measure a set of quantities such as static, dynamic and durability parameters. Among all sensors, only the strain gauges (Fig. 13(a)), inclinometers (Fig. 13(b)) and displacement transducers (Figueiras *et al.* 2010) are considered for this analysis. Moreover, only the first three spans, between piers TP and P3, were selected to carry out this analysis. Fig. 12 and Table 3 summarize the most relevant information about the instrumentation plan for this case.

Concerning the assessment and surveillance of the bridge, a numerical model was implemented based on finite element techniques. Similar to the Sorraia Bridge case, a two-dimensional beam model was adopted to simulate the concrete elements of the bridge.

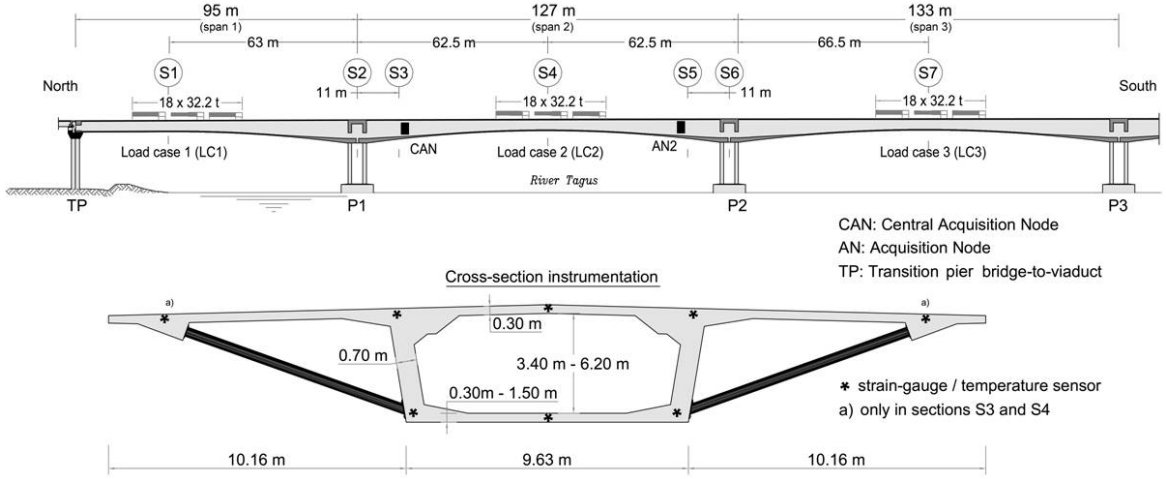

Fig. 12 Location of the instrumented cross-sections in Lezíria Bridge

(a) Electric strain-gauge (b) inclinometer installation (c) Acquisition node

Fig. 13 Monitoring system of Lezíria Bridge

Table 3 Instrumentation typology and quantities – Lezíria Bridge

Parameter	S1	S2	S3	S4	S5	S6	S7
Vertical displacement	1	-	-	1	-	-	1
Rotation	-	1	-	-	-	1	-
Deformation	6	-	8	8	6	-	6
Temperature	2	-	8	8	-	-	2

Similarly to that which was presented for Sorraia Bridge, the vertical displacements were estimated based on measurements collected during the load test performed at the end of construction. Fully loaded trucks were used in order to carry out the load tests, which comprised a set of truck configurations immobilized at positions that caused maximum curvature of mid-span cross-sections. With interest for this analysis, three load cases are explored, namely, Load Cases 1, 2 and 3 (Fig. 12).

The polynomial functions were calculated based on the aforementioned measurements and the intrinsic characteristics of the bridge, namely null vertical displacements above piers and null curvature at the end support of the outer span (span 1).

Fig. 14(a) shows the results for the vertical displacements. In the light of the results, the estimation obtained for cross-section S4 with a 6^{th} degree polynomial function presents a good conformity with the measured one. On the contrary, poorer results were attained for spans 1 and 3, for which a 4^{th} and 3^{rd} degree polynomial function was respectively used. The error lower than 5% obtained for cross-section S4 is a good indicator, taking into account that a polynomial approach was used to assess the real bridge deflection. Again, the different number of instrumented cross-sections for each span can explain these differences in errors, which indicates that the error increases as the polynomial degree decreases. Observing the rotation diagrams in Fig. 14(b), the highest deviations occur again near piers P1 and P2. Focussing on LC1 and LC3, the rotations computed with the polynomial functions seem to be overestimated for spans 1 and 3 near piers P1 and P2, respectively. This might justify the error magnitudes obtained for cross-sections S1 and S7. Moreover, the results for span 3 are completely out of bounds, which can be explained by the few constraints that are known for the girder cross-section above the pier P3. This shows that using only a null vertical displacement in a support cross-section is insufficient to attain acceptable results. Therefore, without additional information about the span behaviour over pier P3, it is not possible to estimate the bridge deflection for span 3 with an acceptable degree of accuracy.

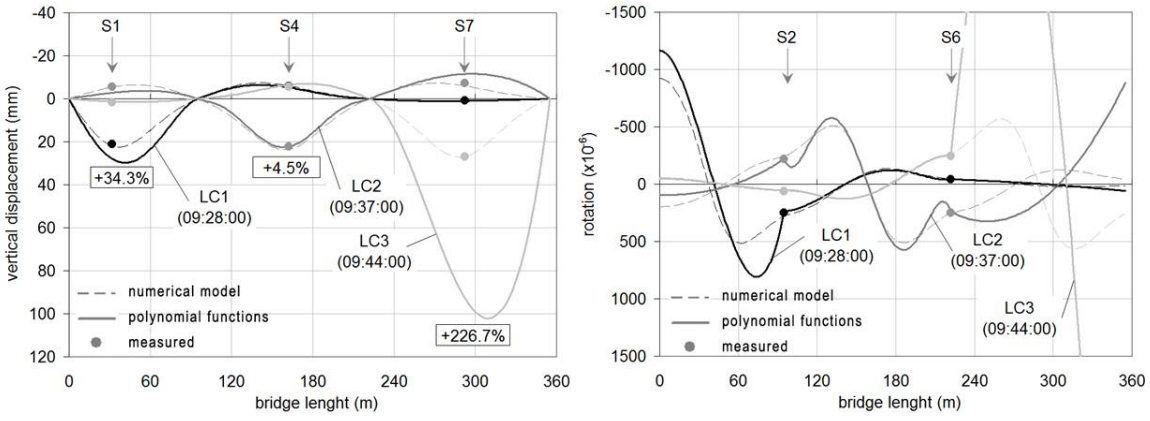

(a) vertical displacement diagrams (b) rotation diagrams

Fig. 14 Lezíria Bridge results for LC1, LC2 and LC3 (case 0)

4. Strategies to improve the evaluation of bridge deflections

4.1 Based on data extrapolation of curvatures

If Figs. 8 and 12 are carefully scrutinized, the two girder cross-sections instrumented near piers S3 and S5 are not exactly above the pier axis but inside of span 2. The preference for these two cross-sections instead of the girder cross-sections over supports S2 and S6 is due to the fact that the deformation field of the latter does not follow the Bernoulli hypothesis. Therefore, cross-sections over supports are avoided in measuring strains because they are not suitable for estimating cross-section curvatures. Hence, only one cross-section instrumented with strain gauges is available for each span, 1 and 3. In spite of the fact that a 4^{th} order polynomial function may be used to estimate the span deflection, the quality of the results obtained for spans 1 and 3 is poor, as previously presented in Figs. 10(a) and 14(a). Therefore, the curvature of cross-sections near the intermediate supports is crucial information for accurate predictions. To overcome this limitation imposed by the monitoring systems, the curvature of these cross-sections was estimated with the polynomial function obtained for span 2 and therefore, the degree of the polynomial functions used for spans 1 and 3 could be incremented by one.

Accordingly, Fig. 15(a) presents the results for Sorraia Bridge, where a considerable improvement is attained for spans 1 and 3. The relative error for cross-sections S1 and S7 decrease from + 12.9% to – 4.5% and from 14.2% to – 1.9%, respectively. As a result, the curvatures of cross-sections S2 and S6, calculated with the polynomial function obtained for span 2, is a valid strategy. Moreover, concerning the rotations, the errors also decrease near piers P1 and P2, as can be confirmed by the rotation diagrams shown in Figs. 10(b) and 15(b).

As far as Lezíria Bridge is concerned, the results for span 3 are not satisfactory due to the scarce information on the deck behaviour over pier P3, as already mentioned. Therefore, the use of the deck curvature over piers, obtained with the polynomial function of span 2, is only applied for cross-section S2 (span 1). Fig. 16(a) shows the vertical displacement results, which are significantly better than the ones presented in Fig. 14(a). The relative error decreases from +34.3% to +3.3% for cross-section S1. The deviations observed for the rotations near piers P1 also decrease, which is the main reason for the improvement in results, as can be confirmed if the rotation diagrams shown in Figs. 14(b) and 16(b) are compared.

The results presented in both Figs. 15 and 16 correspond to specific registers from all that are stored in the database. However, visualization over time is also possible by plotting sequentially the deflection curves calculated for all registers collected during the observation period $[t_{initial},t_{final}]$. Fig. 17 shows the evolution of vertical displacements during the load test for both bridges in cross-sections S1, S4 and S7 (S7 for Sorraia Bridge only). Two results are plotted: (i) calculated with polynomial functions (continuous line), and (ii) the sensor measurements (marker shapes). In general, the computed values and the measured ones exhibit good conformity, namely the trend evolution that is clearly identical. It is worth mentioning that the time window in the Sorraia Bridge case (Fig. 17(a)) includes two other load positions that have not been discussed in the present analysis.

4.2 Based on rotation measurements

Although the vertical displacements are satisfactorily estimated for cross-sections S1, S4 and S7 (error less than 4.5%), the same cannot be said for the deflection curves. Observing the deflection shape near the inner supports P1 and P2 of both bridges (Figs. 15(a) and 16(a)), a deviation of the normal curvature's evolution is clearly visible. Moreover, the deflection curves estimated by the polynomial functions exhibit a higher curvature near the pier supports if compared with the numerical results, as shown in the rotation diagrams presented in Figs. 15(b)

and 16(b). For example, in the LC2 presented in Figs. 15 and 16, an inflection of the deformed shape above pier P1 is clearly noticeable.

On the other hand, strain gauges measure local deformations, which could give unreliable readings to estimate bridge deflections if cracks occur in the instrumented zone. To avoid this problem, long gauges are preferable in order to get average deformations, which is not the case in the examples herein presented. Therefore, the installation of additional inclinometers might be a valid alternative to improve the quality of the estimated deflection shapes. If compared with strain gauges, which are commonly installed before the concrete is poured, with the higher cost and effort of embedded cables in the concrete, inclinometers are easier to install.

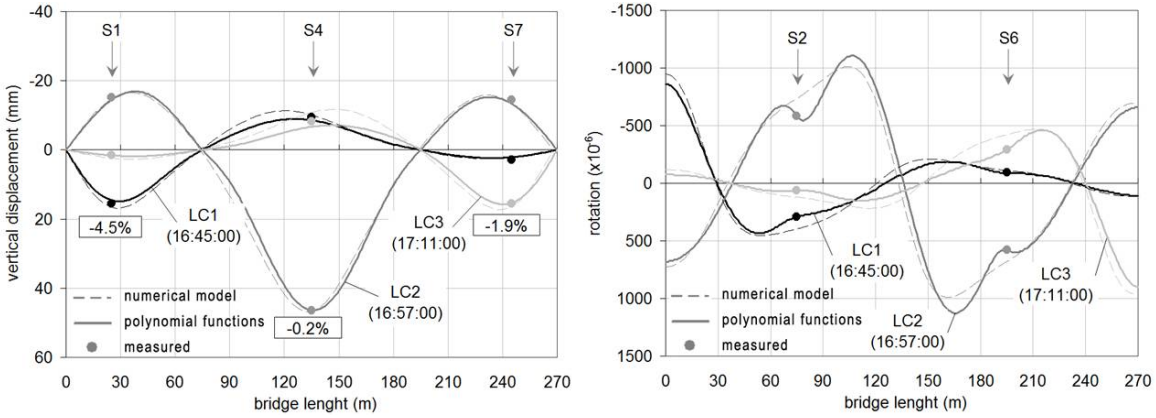

(a) vertical displacement diagrams (b) rotation diagrams

Fig. 15 Sorraia Bridge results for LC1, LC2 and LC3 (case 1)

In this context, the bridge deflection evaluation based on rotations is discussed. Due to the absence of additional field rotation measurements, the subsequent analysis is throughout supported by the numerical results. In order to seek the best fitting for the bridge deflection, a parametric analysis was performed using rotations at different cross-sections. For each span, and accordingly with Fig. 18, two rotations above the piers – fixed inclinometers – and, at variable positions, four inclinometers in the case of inner spans (symmetrically positioned relative to the mid-span cross-section) and two inclinometers in the case of the end spans – movable inclinometers – are considered. The different configuration adopted for the end spans is related to the discontinuity at one of the end cross sections, which is an additional constraint (null curvature) for solving the problem. On the other hand, the shift of the cross-section with maximum vertical displacement to the side of deck discontinuity justifies the adopted inclinometers' positioning. The movable inclinometers were successively moved 5 m apart (approximately 5% inner span length), in order to explore several possible configurations (Fig. 18).

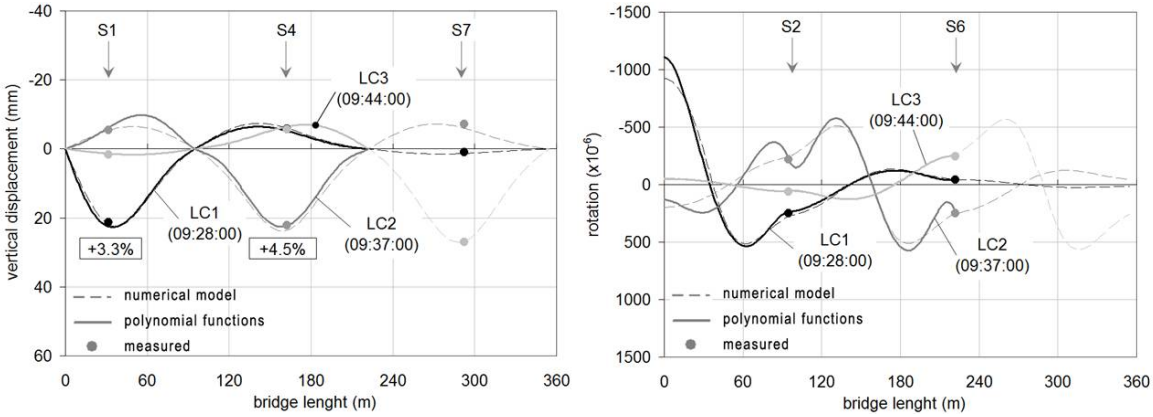

(a) vertical displacement diagrams (b) rotation diagrams

Fig. 16 Lezíria Bridge results for LC1, LC2 and LC3 (case 1)

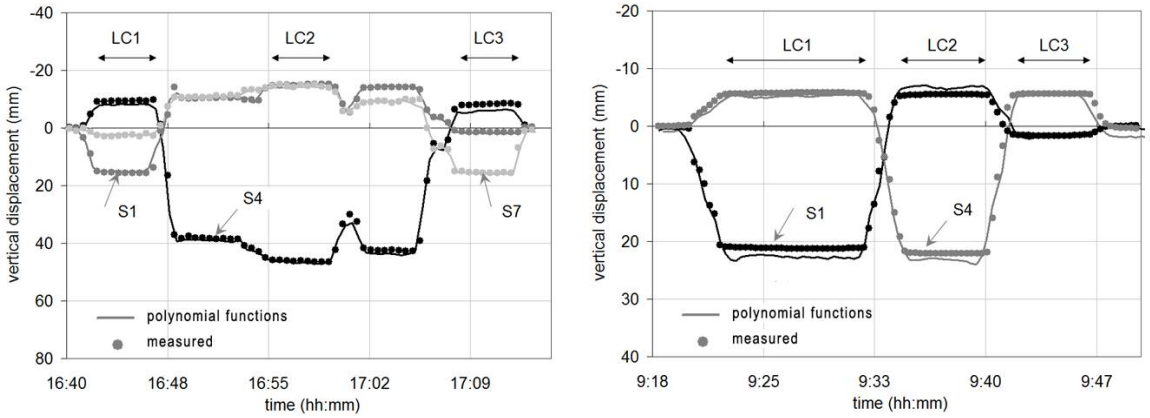

(a) Sorraia Bridge (b) Lezíria Bridge

Fig. 17 Vertical displacement time-series during the load test

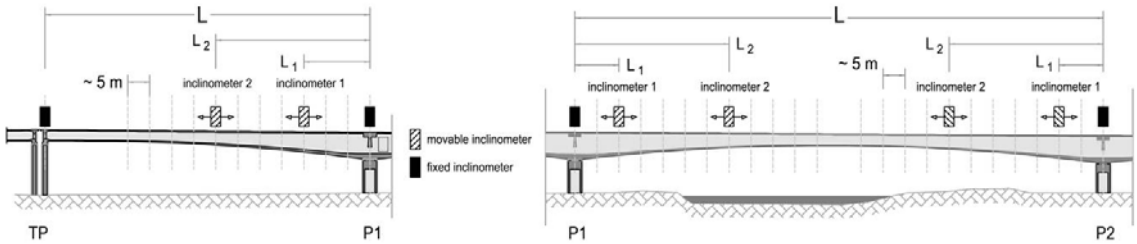

(a) end spans (b) inner spans

Fig. 18 Parametric analysis for the bridge deflection calculation based on rotations

Fig. 19 presents the results of the parametric analysis performed for Sorraia Bridge. For each span, the results show the average error committed, which is calculated as the quotient between the

average of the absolute differences between the vertical deflection calculated by the polynomial function and the one obtained by the numerical model, and the maximum vertical displacement (Eq. (14)). For each pair entry, the column height represents the average error when the inclinometers 1 and 2 are respectively positioned at a distance of $L_1 = \eta_1 \cdot L$ and $L_2 = \eta_2 \cdot L$ of the pier (Fig. 18).

$$e_j = \frac{\sum_{k=1}^{z} \left| \delta_{j,k} - \overline{\delta}_{j,k} \right|}{z} \Big/ \max \left| \overline{\delta}_{j,k} \right| \quad , \quad \begin{cases} \delta_{j,k} - \textit{polynomial function} \\ \overline{\delta}_{j,k} - \textit{numerical model} \end{cases} \tag{14}$$

The results show that the optimal position for inclinometers 1 and 2 are at $L_1 = 0.14 \cdot L$ and $L_2 = 0.42 \cdot L$ in the case of the end spans, while for the inner spans the optimal positions are at $L_1 = 0.12 \cdot L$ and $L_2 = 0.30 \cdot L$. As Fig. 19 indicates, the average errors are about 1% for the three spans, which corresponds to a local minimum.

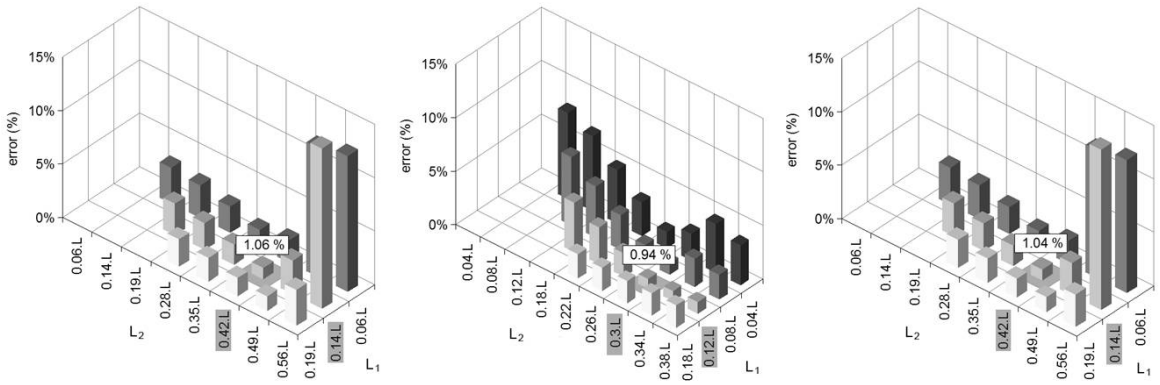

(a) span 1 (b) span 2 (c) span 3

Fig. 19 Results of the parametric analysis for Sorraia Bridge

Considering these optimal positions for the inclinometers, Fig. 20(a) shows the bridge deflection estimation that exhibits a close agreement with the results from the numerical model and the measured ones. The rotation diagrams presented in Fig. 20(b) also exhibit good conformity, with slight deviations near piers P1 and P2 that might be explained, again, by the higher variation of the cross-section inertia in these zones. For cross-sections S1, S4 and S7, the relative error, between the value predicted by the polynomial function and that by the numerical model is less than 2%.

Regarding the Lezíria Bridge case, the results from the parametric analysis are shown in Fig. 21. The optimal position of the inclinometers 1 and 2 are at $L_1 = 0.15 \cdot L$ and $L_2 = 0.41 \cdot L$ for end spans, while for inner spans the best positions are at $L_1 = 0.11 \cdot L$ and $L_2 = 0.31 \cdot L$. For the three spans, the average errors are approximately 1.4%, corresponding in all to a local minimum as can be observed in Fig. 21.

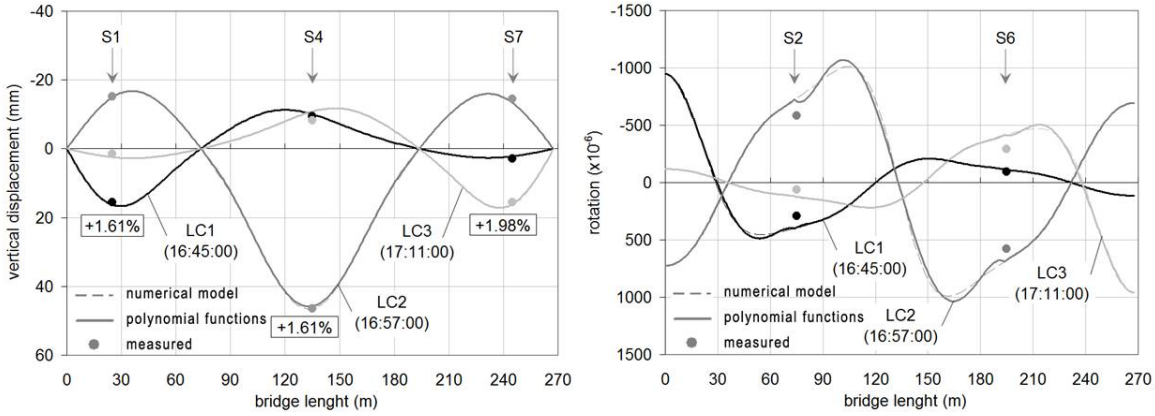

(a) vertical displacement diagrams (b) rotation diagrams

Fig. 20 Sorraia Bridge results for LC1, LC2 and LC3 (case 2)

Based on these optimal positions for the inclinometers, Fig. 22(a) shows the bridge deflection obtained, in which an almost perfect agreement is observed between data. The rotation diagram presented in Fig. 22(b) also exhibits good conformity, with slight deviations near the piers P1 and P2, which can again be explained by the higher variation of cross-section inertia in these zones. For cross-sections S1, S4 and S7, the relative error, between the value predicted by the polynomial function and that by the numerical model is less than 3%.

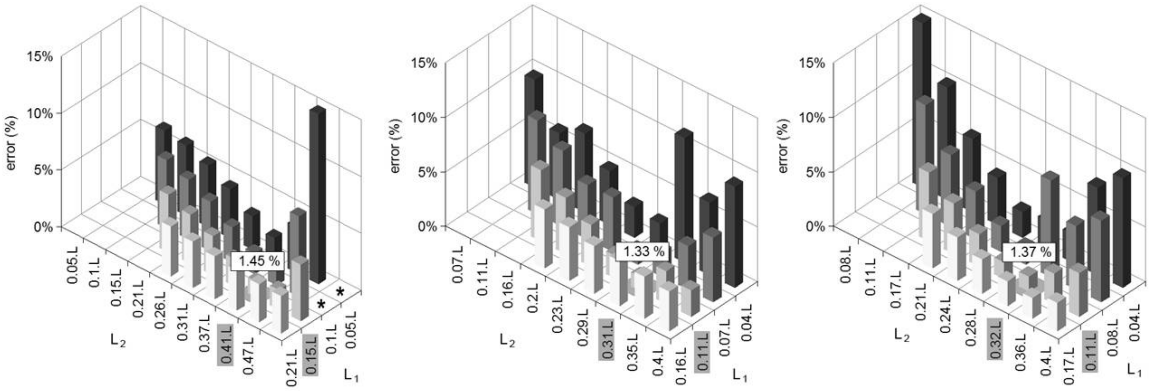

(a) span 1 (b) span 2 (c) span 3

* error > 15 %

Fig. 21 Results of the parametric analysis for Lezíria Bridge

The similar patterns achieved for the bridge deflection calculated with the polynomial functions and the numerical model is the most relevant improvement. If the results of both bridges are compared, the relative location of the movable inclinometers is practically the same for both bridges, which is also very important to note. Therefore, taking into account these results, Fig. 23 draws the optimal configuration for the inclinometers positioning with the purpose of estimating

the bridge deflection: (i) four inclinometers for end spans and (ii) six inclinometers for inner spans.

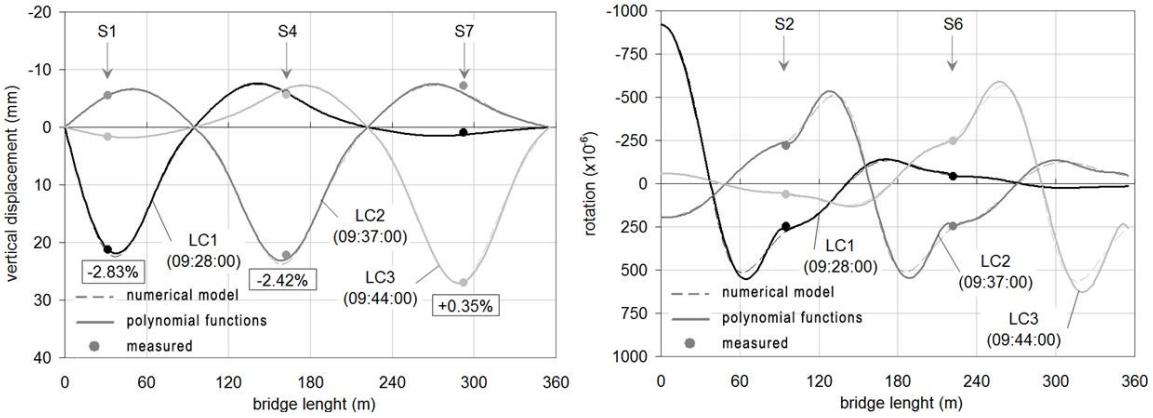

(a) vertical displacement diagrams (b) rotation diagrams

Fig. 22 Lezíria Bridge results for LC1, LC2 and LC3 (case 2)

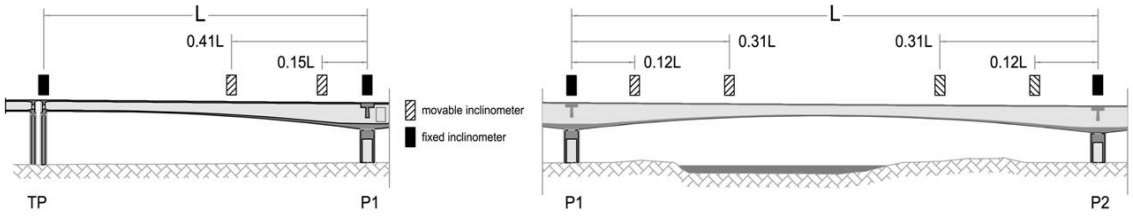

(a) extreme spans (b) inner spans

Fig. 23 Optimal positioning of the inclinometers to estimate the bridge deflection

5. Conclusions

The present work focuses on the evaluation of bridge deflections based on polynomial functions using strain and rotation measurements. The procedure to estimate the bridge deflections is presented and applied to a prestressed concrete beam and two full-scale bridges built using the balanced cantilever method – the Sorraia Bridge and the Lezíria Bridge. The results are compared with the sensor measurements and those obtained by applying suitable bridge numerical models. Some relevant conclusions could be drawn:

1. The data processing is a computationally heavy task, namely if long periods of observation are handled. However, software implementation, such as the one provided by MENSUSMONITOR, revealed to be efficient and flexible for data input/output. The time spent in data handling was significantly shortened, if compared with traditional tools such as spreadsheets. Moreover, it offers the advantage of making real time visualization possible by directly connecting to acquisition systems or monitoring databases.
2. The procedure herein described was first applied to a simply supported beam subjected to two different load cases. Satisfactory results were attained with a maximum relative error of 4.9%.
3. Concerning the full-scale bridges, the spans with the highest number of instrumented

cross-sections, i.e. span 2 in the examples, exhibit the best results with errors below 4.5% for the cross-section located at mid-span. These results show that a 6th degree polynomial function, based on three cross-sections instrumented with strain gauges and two cross-sections instrumented with inclinometers, can satisfactorily predict the vertical displacement of the mid-span cross-section.

4. The consideration of the curvatures above piers P1 and P2, extrapolated from the polynomial function determined for span 2, led to an improvement of the quality of results with relative errors lower than 4.5% for the vertical displacements of the adjacent spans. In this case, good results can be attained with a 5th degree polynomial function, derived from three curvatures and one rotation.

5. The bridge deflections calculated with the polynomial functions deviate slightly from the results obtained with the numerical model, namely because of the unsatisfactory results obtained for the rotations near the support piers. However, the initial aim of the instrumentation plans was not the estimation of the deflection curves with polynomial functions. Furthermore, the real bridge deflection is a rational type function instead of a polynomial type, which is a critical aspect near the supports due to the high variation of inertia that can negatively affect the approximation with a polynomial function. Nevertheless, the estimated deflections present a satisfactory conformity with the ones obtained with the numerical models.

6. An alternative approach using inclinometer measurements was numerically tested. A parametric analysis was performed, with several configurations that comprised four inclinometers for the end spans and six inclinometers for the inner spans. The optimal solution conducted to a maximum relative error lower than 3%, and a perfect matching of patterns was achieved between the bridge deflection computed with the polynomial functions and the one obtained by the numerical model. Based on rotation measurements, suitable results might be achieved with a 5th and a 7th degree polynomial function for the end and the inner spans, respectively.

7. Regarding the evaluation of the bridge deflection based on rotation measurements, the obtained results allowed for the definition of the relative position of the inclinometers for both bridges erected using the balanced cantilever method.

Acknowledgements

The authors gratefully acknowledge the financial support provided by the Portuguese Foundation for Science and Technology (FCT-MCES) to the first and second authors through the PhD grants SFRH/BD/29125/2006 and SFRH/BD/42315/2007, respectively.

References

Björck, A. (1996), *Numerical methods for least squares problems*, Philadelphia : Society for Industrial and Applied Mathematics.

BRITE/EURAM (1997), *SMART STRUCTURES – Integrated Monitoring Systems for Durability Assessment of Concrete Structures*, Project Nº BRPR-CT98-0751.

Burdet, O. and Zanella, J.L. (2000), *Automatic monitoring of bridges using electronic inclinometers*, *IABSE*, Lucerne Congress Structural Engineering for Meeting Urban Transportation Challenges, IABSE, Lucerne Congress Structural Engineering for Meeting Urban Transportation Challenges: 398-399.

Cavadas, F. and Oliveira, P. *et al.* (2009). *Análise da resposta estrutural de uma viga de betão armado e pré-esforçado, simplesmente apoiada, face a duas cargas pontuais (internal report)*, Porto, LABEST, Faculty of Engineering of the University of Porto.

Chung, W., Kim, S., Kim, N.S. and Lee, H.U. (2008), "Deflection estimation of a full scale prestressed concrete girder using long-gauge fiber optic sensors", *Constr. Build. Mater.*, **22**(3), 394-401.

Figueiras, J. and Félix, C. *et al.* (2010), *Transducer for mesuring vertical displacements*, Universidade do Porto and Instituto Politécnico do Porto. WO/2010/053392. Portugal.

Hou, X., Yang, X. And Huang, Q. (2005), "Using inclinometers to measure bridge deflection", *J. Bridge Eng.*, **10**(5), 564-569.

Massonnet, C. (1968), *Résistance des matériaux*. Paris, Dunod.

Perdigão, V. and Barros, P. *et al*. (2006), "Development and implementation of a long term structural health monitoring", *Proceedings of the IABMAS'06 – 3rd International Conference on Bridge Maintenance, Safety and Management*, Porto, Portugal.

Sousa, H. (2002), *Comportamento de uma viga de betão armado e pré-esforçado em modelo reduzido*, Estágio do PRODEP III. Porto, Engineering Faculty, University of Porto.

Sousa, H., Dimande, A. *et al*. (2008), "MENSUSMONITOR – Tool for the treatment and interpretation of experimental results in Civil Engineering", *CCC 2008 – Challenges for Civil Construction*, FEUP - Faculty of Engineering, University Porto, Porto, FEUP.

Sousa, H., Felix, C., Bento, J. and Figueiras, J. (2011), "Design and implementation of a monitoring system applied to a long-span prestressed concrete bridge", *Struct. Concrete*, **12**(2), 82-93.

Sousa, H., Matos, J. and Figueiras, J. (2006), "Development of an embedded sensor holder for concrete structures monitoring", *Proceedings of the 2nd Congress fib*, Naples, Italy.

Van der Auweraer, H. and Peeters, B. (2003), "International research projects on structural health monitoring: an overview", *Struct. Health Monit.*, **2**(4), 341-358.

Vurpillot, S., Krueger, G., Benouaich, D., Clement, D. and Inaudi, D. (1998), "Vertical deflection of a pre-stressed concrete bridge obtained using deformation sensors and inclinometer measurements", *ACI Struct. J.*, **95**(5), 518-526.

CC